# Constant-stress nonequilibrium molecular dynamics: Shearing of the soft-sphere crystal and fluid

D. Brown and J. H. R. Clarke
*Chemistry Department, The University of Manchester Institute of Science and Technology, Manchester M60 1QD, England, United Kingdom*
(Received 10 March 1986)

A new method is described for studying shear flow in fluids and crystals using nonequilibrium molecular dynamics (NEMD) based on determining the response of the system to a predetermined homogeneous shear stress. Flow phenomena may be examined which would not be accessible using other techniques. We demonstrate the existence of a yield stress for shear along the (111) plane of an ideal (i.e., defect-free) fcc soft-sphere crystal. The significant differences with previous simulation results using constant strain rate NEMD are discussed in terms of artifacts introduced by sample size effects and crystal geometries in relation to the direction of shear.

## INTRODUCTION

Previous measurements of the shear viscosity of fluids by nonequilibrium molecular dynamics (NEMD) have been made by imposing a shear rate of predetermined time and space dependence and then measuring the response of the appropriate component of the stress tensor.[1-3] Recent developments[4] have led to the possibility of inverting this procedure to measure the viscosity by applying a predetermined fixed shear stress to the system and observing the fluctuations in the shear rate.

The main aims of this paper are to show that while the constant-stress method gives essentially identical results to constant strain rate for liquids it offers important advantages for studying the shear of highly viscous and solid materials. This is illustrated by applying stress to a sample of the face-centered-cubic (fcc) soft-sphere crystal. At low applied stress the crystal strains as a solid with a distinct zero-frequency shear modulus $G_0$. At higher applied stresses the sample first "yields" and then flows with at least two discernible "fluid" phases linked by a distinct phase transition. These flow phenomena would not be accessible using the Rahman-Parinello constant-stress method.[5] If spurious effects can be eliminated by appropriate choice of sample size and boundary conditions the method offers wider opportunities for studying flow phenomena.

We also describe the equations of motion for constant stress and outline an algorithm for use in NEMD simulations. The method to be described is the off-diagonal analogue of Evans and Morriss's[4] technique for performing isothermal-isobaric molecular dynamics.

## METHOD

The starting point for this method is the following equations of motion[4,6] for isothermal planar Couette flow in the $xz$ plane:

$$\dot{\mathbf{q}}=\mathbf{p}/m+q_z\dot{\gamma}\hat{x}\ , \tag{1}$$

$$\dot{\mathbf{p}}=\mathbf{F}-\alpha\mathbf{p}-\dot{\gamma}p_z\hat{x}\ , \tag{2}$$

where $\hat{x}$ is the unit vector in the $x$ direction. $\alpha$ and $\dot{\gamma}$ are treated as undetermined parameters and are evaluated from the constraints applied to the system. Firstly, we require that the total kinetic energy of the system,

$$K_e=\tfrac{1}{2}\sum_{i=1}^{N}\mathbf{p}_i^2/m\ ,$$

remains fixed. This means that $\dot{K}_e=0$ and implies that

$$\sum\mathbf{p}\cdot\dot{\mathbf{p}}=0\ ,$$

where for simplicity we have assumed all particles have the same mass $m$, and unless specified $\sum$ indicates a sum over all $N$ particles. Substituting for $\dot{\mathbf{p}}$ gives the value of $\alpha$ required to satisfy the constraint

$$\alpha=\left[\sum\mathbf{p}\cdot\mathbf{F}-\dot{\gamma}\sum p_xp_z\right]\Big/\sum\mathbf{p}^2\ . \tag{3}$$

The second constraint is to specify the rate of change of the $xz$ component of the stress tensor, $\dot{\sigma}_{xz}$. $\sigma_{xz}$ is defined by

$$-V\sigma_{xz}=\sum(p_xp_z/m+q_xF_z)\ , \tag{4}$$

where $V$ is the volume of the system, so differentiating with respect to time gives

$$-V\dot{\sigma}_{xz}=\sum(1/m)(p_x\dot{p}_z+\dot{p}_xp_z)+\sum(\dot{q}_xF_z+q_x\dot{F}_z)\ . \tag{5}$$

Substituting for $\dot{\mathbf{p}}$ and $\dot{\mathbf{q}}$ from Eqs. (1) and (2) and rearranging leads to

$$\dot{\gamma}=\frac{\sum[(1/m)(2p_xF_z+F_xp_z-2\alpha p_xp_z)+q_x\dot{F}_z]+\dot{\sigma}_{xz}V}{\sum(p_z^2/m-q_zF_z)-2\left[\sum p_xp_z\right]^2\Big/m\sum\mathbf{p}^2}\ , \tag{6}$$

Further substitution for $\alpha$, Eq. (3), gives

 

$$\dot{\gamma}=\frac{\sum(1/m)(2p_xF_z+F_xp_z)-\frac{2}{m}\frac{\sum\mathbf{p}\cdot\mathbf{F}\sum p_xp_z}{\sum\mathbf{p}^2}+\sum q_x\dot{F}_z+\dot{\sigma}_{xz}V}{\sum(p_z^2/m-q_zF_z)-2\left[\sum p_xp_z\right]^2\Big/m\sum\mathbf{p}^2}\ . \tag{7}$$

The term involving $\dot{F}_z$ involves the second differential of the potential so a further substitution has to be made. Firstly, it is assumed that the particles interact through a pairwise additive potential $\Phi(r)$, a function only of their separation $r=|\mathbf{q}_{ij}|$ where $\mathbf{q}_{ij}=\mathbf{q}_i-\mathbf{q}_j$. The force on particle $i$ due to $j$ is then given by

$$\mathbf{F}_{ij}=-\frac{d\Phi(r)}{dr}\hat{\mathbf{q}}_{ij}=-\Phi'\hat{\mathbf{q}}_{ij}\ .$$

The term involving $\dot{F}_z$ can now be converted into a double sum ($\sum\sum$ implies $\sum_{i=1}^{N-1}\sum_{j>i}^{N}$)

$$\sum q_x\dot{F}_z=\sum\sum q_{x_{ij}}\dot{F}_{z_{ij}}=\sum\sum q_{x_{ij}}\frac{d(-\Phi'\hat{q}_{z_{ij}})}{dt}\ . \tag{8}$$

Evaluation of the differential in Eq. (8) introduces yet another term in $\dot{\gamma}$ and after some tedious yet straightforward algebra one arrives at the final equation

$$\dot{\gamma}=\left\{\sum(1/m)(2p_xF_z+F_xp_z)-\frac{2}{m}\frac{\sum\mathbf{p}\cdot\mathbf{F}\sum p_xp_z}{\sum\mathbf{p}^2}+\dot{\sigma}_{xz}V-\sum\sum\left[\frac{q_{x_{ij}}p_{z_{ij}}}{m}\frac{\Phi'}{|\mathbf{q}_{ij}|}+\frac{(\mathbf{q}_{ij}\cdot\mathbf{p}_{ij}/m)q_{x_{ij}}q_{z_{ij}}}{\mathbf{q}_{ij}^2}\left[\Phi''-\frac{\Phi'}{|\mathbf{q}_{ij}|}\right]\right]\right\}$$
$$\times\left\{\sum\frac{p_z^2}{m}-\frac{2(\sum p_xp_z)^2}{m\sum\mathbf{p}^2}+\frac{\sum\sum q_{x_{ij}}^2q_{z_{ij}}^2}{\mathbf{q}_{ij}^2}\left[\Phi''-\frac{\Phi'}{|\mathbf{q}_{ij}|}\left[1-\frac{\mathbf{q}_{ij}^2}{q_{x_{ij}}^2}\right]\right]\right\}^{-1}\ . \tag{9}$$

In this form $\dot{\gamma}$ can be readily calculated from quantities either stored or evaluated in the normal MD procedure with the addition of $\Phi''$.

## IMPLEMENTATION

As with other methods for simulating planar shear flow the equations of motion are integrated in conjunction with the moving boundary scheme of Lees and Edwards (see Ref. 4). We find that the integration of the coupled first-order differential equations presents no problems if fourth-order Gear predictor-corrector methods[4] are used but there are some extra considerations concerning the moving boundaries due to the fluctuating shear rate.

If at time $t=0$ the periodic images are orthogonal then at a later time $t$ the distance moved by the image cell, $h(t)$, is given by

$$h(t)=\int_0^t\dot{\gamma}(s)L\,ds\ , \tag{10}$$

where $L$ is the length of the MD cell in the $z$ direction. In the case of the constant-strain-rate NEMD $\dot{\gamma}$ is constant so that $h(t)=\dot{\gamma}Lt$. In the present case, however, the shear rate is a function of time so the evaluation of $h(t)$ is more complicated. A convenient way of doing this is to reformulate Eq. (10) as a differential equation

$$\dot{h}(t)=\dot{\gamma}(t)L \tag{11}$$

and then use the Gear fourth-order predictor-corrector scheme to solve for $h(t)$. This is a useful procedure since the higher derivatives of $\dot{\gamma}$ are also required when a particle crosses a $z$ boundary. Consider the displaced periodic image of a particle, $\mathbf{q}'$, in the $+ve$ $z$ direction. Since $q_x'=q_x+h$, differentiating with respect to time gives

$$\dot{q}_x'=\dot{q}_x+\dot{h}$$

which from Eq. (11) is

$$\dot{q}_x'=q_x+\dot{\gamma}L\ .$$

Repeated differentiation gives

$$\frac{d^2q_x'}{dt^2}=\frac{d^2q_x}{dt^2}+\frac{d^2\gamma}{dt^2}L\ ,$$
$$\frac{d^3q_x'}{dt^3}=\frac{d^3q_x}{dt^3}+\frac{d^3\gamma}{dt^3}L\ ,$$
$$\frac{d^4q_x'}{dt^4}=\frac{d^4q_x}{dt^4}+\frac{d^4\gamma}{dt^4}L\ ,$$

etc. As $\dot{\gamma}$ is a function of time, $\ddot{\gamma}$ and the higher derivatives are generally nonzero. If a particle moves out of the

primary cell through a $z$ face then not only do its position and velocity change to that of its periodic image, $\mathbf{q}'$, but also all the higher derivatives used in the integration scheme.

## SIMULATIONS

It is expedient to choose a potential which is continuous up to the second derivative and goes smoothly to zero at the chosen cutoff, otherwise discontinuities in the force cause sudden steps in the stress as particles move in and out of their interaction spheres with a resultant drift of the stress away from the required value. Interactions were therefore defined by a soft-sphere potential modified according to a prescription due to Andrea *et al.*[7]

$$\Phi(r)=\begin{cases}4\epsilon(\sigma/r)^{12}, & r\le r_m\\ U(r^2), & r_m<r\le r_c\end{cases}$$

where $U(r^2)=\sum_{i=1}^{6}C_{i-1}\delta^{i-1}$ is a fifth-order polynomial in $\delta=r^2-r_m^2$. The coefficients $C_0,C_1,C_2,\ldots$ were chosen such that the potential and its first two derivatives are continuous at $r_m$ and go to zero at $r_c$. The values of $r_m$ and $r_c$ used were $1.5\sigma$ and $2.3\sigma$, respectively.

The coupled first-order equations of motion, Eqs. (1), (2), and (11), were integrated for a system of $N=504$ particles using a fourth-order Gear predictor-corrector scheme[4] with a reduced time step $[\Delta t^*=\Delta t\,\sigma^{-1}(m/\epsilon)^{1/2}]$ of $\sim 0.001$.

## RESULTS: SOFT-SPHERE LIQUID

We have compared the results from constant-stress and constant-strain-rate simulations with those already obtained for an $N=108$ unmodified soft-sphere system by Evans.[8] Initially the system was equilibrated, $\dot\gamma$ set equal to zero, at a reduced density $(\rho^*=N\sigma^3/V)$ of 0.7 and a reduced temperature $(T^*=Tk_b/\epsilon)$ of 1.0. To "drive" the system to the desired stress $\sigma_r$, $\dot\sigma_{xz}$ was set equal to a relatively small value $\sigma_r/\Delta t=10^{-2}\rightarrow 10^{-3}$ and the simulation started, having first set the kinetic energy to the desired value by scaling the momenta, with $\dot\gamma$ being evaluated from Eq. (9). Once the stress had exceeded $\sigma_r$, $\dot\sigma_{xz}$ was set equal to zero. Attempts to achieve a desired stress in a single time step result in excessive shear rates and consequent instabilities. It was found for this system that the constraints of constant kinetic energy and constant stress were maintained to at least the first seven significant figures. After a period of equilibration at $\sigma_r$, $\sim 1000\Delta t$, averages were obtained over a further $8000\Delta t$. The mean shear rate calculated from this run was then used as input to a second simulation, starting from the same equilibrated configuration, with $\dot\gamma$ fixed at this value. Averages were then obtained for the same number of time steps and the results are given, along with those from Ref. 8, in Table I. The viscosity has been calculated in the usual way from the ratio of the mean stress to mean shear rate

$$\eta=\langle\sigma_{xz}\rangle/\langle\dot\gamma\rangle \tag{12}$$

and also from the $\alpha$ parameter

$$\eta=2\langle\alpha\rangle\langle K_e\rangle/\langle\dot\gamma\rangle^2V\ . \tag{13}$$

Although these equations do not give independent estimates of the viscosity they do provide a useful consistency check. In Table I the soft-sphere scaling procedure has been used to present our results. The following definitions are used for the reduced pressure $(p^*)$, stress $(\sigma_{xz}^*)$, viscosity $(\eta^*)$, and shear rate $(\dot\gamma^*)$:

$$p^*=pV/Nk_bT\ ,$$
$$\sigma_{xz}^*=\sigma_{xz}V/Nk_bT\ ,$$
$$\eta^*=\eta\sigma^2(m\epsilon)^{-1/2}(\epsilon/k_bT)^{2/3}\ ,$$
$$\dot\gamma^*=\tfrac{1}{2}\dot\gamma\sigma(m/\epsilon)^{1/2}(\epsilon/k_bT)^{7/12}\ .$$

The factor of $\frac{1}{2}$ appears in the expression for $\dot\gamma^*$ since Evans defines $\gamma=\frac{1}{2}du_x/dy$, a point which has been overlooked in recent papers.[10,11] For $T^*=1.0$, $\eta$ and $\dot\gamma$ are reduced by the same factors as in Ref. 8.

From Table I it can be seen that the methods give viscosities which agree to within the statistical errors. The similarity of the calculated standard errors indicates that there is nothing to be gained in terms of precision by using the constant-stress method. Computationally it is more complicated and the evaluation of the extra terms

TABLE I. Constant-stress and constant-shear-rate data for the soft-sphere fluid. The reduced density $(\rho^*)$, temperature $(T^*)$, mean pressure $(p^*=pV/Nk_bT)$, mean stress $(\sigma_{xz}^*=\sigma_{xz}V/Nk_bT)$, mean shear rate $[\dot\gamma^*=\frac{1}{2}\dot\gamma\sigma(m/\epsilon)^{1/2}(\epsilon/k_bT)^{7/12}]$, and resultant viscosity $[\eta^*=\eta\sigma^2(m\epsilon)^{-1/2}(\epsilon/k_bT)^{2/3}]$ determined from the stress and from the $\alpha$ parameter $(\eta_\alpha^*)$ for the simulations at (a) constant stress and (b) constant shear rate. The errors quoted are the standard errors determined by the method described by Fincham (Ref. 9). The numbers in parentheses are results from a constant-shear-rate simulation given in Ref. 8.

| | $\rho^*$ | $T^*$ | $p^*$ | $\sigma_{xz}^*$ | $\dot\gamma^*$ | $\eta^*$ | $\eta_\alpha^*$ |
|---|---|---|---|---|---|---|---|
| (a) | 0.7 | 1.0 | 13.89 | 1.808 | 0.376 | 1.68 | 1.67 |
| | | | ±0.03 | | ±0.010 | ±0.04 | ±0.11 |
| (b) | 0.7 | 1.0 | 13.89 | 1.746 | 0.376 | 1.63 | 1.64 |
| | | | ±0.03 | ±0.040 | | ±0.04 | ±0.10 |
| | (0.7) | (1.0) | (14.13) | (1.806) | (0.4) | (1.58) | |

[in Eq. (9)] increased the central processing unit (CPU) time by ~25% for this particular system. However, as we shall demonstrate, the constant-stress method has definite advantages for studying the effects of shear stress on solids.

It can also be seen from Table I that the viscosity evaluated from $\alpha$ is in good agreement with that obtained from the stress, confirming the consistency of the equations of motion. All the results are in good agreement with those of Evans[8] considering the differences in the potential, number of atoms, and the shear rate.

## RESULTS: SOFT-SPHERE CRYSTAL

We have measured the response of a fcc soft-sphere crystal to stress applied parallel to a line of atoms in the (111) plane. As the experiment is carried out at constant stress it should reveal directly the existence of a yield point in this material. It must be emphasized that these simulations are carried out on small samples of an ideal (i.e., defect-free) crystal. Hence any value for a yield stress is likely to be much higher than at the onset of plastic flow in real crystals, a phenomenon which is known to proceed by the creation and motion of defects.[12,13] The main purpose of this paper is to present a comparison with previous simulation data on an ideal system. No attempt is made to compare results with plastic flow in real macroscopic crystals.

Evans[14] has reported results for a constant rate of strain applied to a system of 108 soft spheres at the soft-sphere scaling density, $X=\rho\sigma^3(\epsilon/k_bT)^{1/4}$, of 0.95, for which the equilibrium state is the crystal. The data obtained were interpreted in terms of three distinct shear-induced fluid phases with the high-shear-rate phase being that of the normal shearing metastable fluid. This was described as an example of shear-induced melting. Although it was claimed that the soft-sphere crystal behaves as a Bingham plastic it is not possible to determine directly a yield stress from a constant-shear-rate NEMD experiment as the crystal is forced to undergo shear flow even for the smallest shear rate. It has been suggested[15] that the phase transitions and shear-induced melting observed by Evans[14] are artifacts introduced by shearing a small periodic system in an unfavorable orientation. Although the orientation of shear with respect to the crystal lattice is not stated in Ref. 14 it is assumed from the system size ($N=108$) and as there is no mention of noncubicity of the MD cell that the shear was directed along the (100) face of a face-centered-cubic crystal. The most likely stable shearing plane, however, is probably the (111) face.[15] A simple geometric analysis reveals that, even allowing for lateral movement of the layers, the displacement barriers to the movement of one plane of atoms over another along these two faces are approximately three times lower in the case of the (111) face.

The crystal sample was set up with $N_z$ close-packed layers of $N_xN_y$ atoms packed together in the *ABC* formation required for a fcc crystal, where $N_xN_yN_z=7\times8\times9=504=N$. The $x$ direction lays parallel to the line of atoms in the $xy$ plane and the ratio of the orthorhombic MD cell dimensions were then $N_xa:N_y(\sqrt{3}/2)a:N_z(\sqrt{2}/\sqrt{3})a$ where $a$ is the nearest-neighbor separation and is equal to $2^{1/6}\sigma$ for $\rho^*=1.0$. This system was then equilibrated at the soft-sphere scaling density of $X=0.95$ for $9000\Delta t$. Averages were then obtained at equilibrium under isokinetic conditions by integrating Eqs. (1) and (2) with $\dot\gamma$ set equal to zero.

The crystal system was subjected successively to stresses ($\sigma^*_{xz}$) of magnitude ~0.56, 1.13, and 1.71, using the method already described. All of these levels of stress were supported without shearing, in each case, for times in excess of $10^4\Delta t$. Upon further increasing the stress to ~2.28, however, the crystal was observed to undergo shear. To pinpoint more precisely the yield stress, calculations at four more stress levels were performed, each starting from the strained configuration at $\sigma^*_{xz}\sim1.71$. Results from all these are given in Table II.

It is interesting to note from Table II that the application of stresses just in excess of the yield point leads to significant metastable behavior. At $\sigma^*_{xz}=1.776$ the crystal supported the stress for a time of $\sim12\,000\,\Delta t^*$ before yielding rapidly to give a stable shearing phase. The behavior at a slightly higher stress of $\sigma^*_{xz}=1.848$ is illustrated in Fig. 1 where the distance the periodic images have moved $h^*(t)=h(t)/\sigma$ [see Eq. (10)] has been plotted against time. At short times, $<2500\Delta t$, $h(t)$ is reasonably constant indicating that the crystal is straining only. The crystal then yields and flows at a relatively slow rate before undergoing a transition at around $15\,000\,\Delta t$ to a second shearing phase.

In Fig. 2 the mean shear rate is plotted as a function of the applied stress for all the simulations given in Table II. The metastable points are distinguished by the diamonds. It can be seen that the sample exhibits a distinct yield stress $\sigma^{0*}_{xz}=1.74\pm0.03$. Also given in Fig. 2 is the constant-shear-rate data of Evans,[14] nominally for the same system. Clearly there are significant differences between the two sets of results. We note that extrapolation of Evans's data implies a yield stress about half our observed values whereas a *higher* value is expected on the basis of the different orientations of the crystal with respect to the shear. In an ideal, (i.e., defect-free) crystal simple theoretical models suggest that the yield stress should be about an order of magnitude less than the infinite-frequency shear modulus $G_\infty$. The latter quantity can be evaluated from the equilibrium stress fluctuations[16]

$$G_\infty=\langle\sigma^2_{\alpha\beta}(0)\rangle V/k_bT,\quad \alpha,\beta=x,y,z\ .$$

The value obtained was $G^*_\infty=13.3\pm1.4$ which is about eight times larger than the yield stress. This is well within the range of simple theoretical predictions.[17]

Our data exhibit at least three distinct stress-dependent phases. At applied stresses below the observed yield stress the crystal strains as an elastic solid. This behavior can be generally described by the equation

$$\sigma_{xz}=G_0\gamma\ , \tag{14}$$

where $G_0$ is a shear modulus and $\gamma$ is the *strain* which for the geometry used here is given by [see Eq. (10)]

$$\gamma=h(t)/L\ .$$

TABLE II. Constant-stress and equilibrium data for the soft-sphere crystal. The (111) direction is in the $xy$ plane. The reduced mean stress ($\sigma_{xz}^* = \sigma_{xz}V/Nk_bT$), mean shear rate [$\dot{\gamma}^* = \frac{1}{2}\dot{\gamma}\sigma(m/\epsilon)^{1/2}(\epsilon/k_bT)^{7/12}$], resultant viscosity [$\eta^* = \eta\sigma^2(m\epsilon)^{-1/2}(\epsilon/k_bT)^{2/3}$], and mean pressure ($p^* = pV/Nk_bT$) determined from the equilibrium and constant-stress simulations at the soft-sphere scaling density $X = \rho^*(\epsilon/k_bT)^{1/4}$ of 0.95. $N_s$ and $N_a$ are the total number of time steps and the number of time steps over which averages were taken at each value of $\sigma_{xz}$, respectively. The points bracketed together showed clear evidence of metastable behavior for the fixed value of the stress. In each case the lower figures represent those of the more stable state.

| $\sigma_{xz}^*$ | $\dot{\gamma}^*$ | $\eta^*$ | $p^*$ | $N_s$ | $N_a$ |
|---|---|---|---|---|---|
| −0.007 | 0 | | 26.40 | 25 800 | 16 800 |
| ±0.019 | | | ±0.01 | | |
| 0.561 | ~0 | | 26.44 | 12 000 | 8000 |
| | | | ±0.02 | | |
| 1.133 | ~0 | | 26.55 | 12 800 | 8800 |
| | | | ±0.02 | | |
| 1.705 | ~0 | | 26.70 | 11 200 | 7200 |
| | | | ±0.02 | | |
| [1.776 | ~0 | | 26.74 | 25 600 | 10 400 ] |
| | | | ±0.02 | | |
| [1.776 | 0.059 | 23.21 | 26.82 | 25 600 | 11 200 ] |
| | ±0.009 | ±3.49 | ±0.06 | | |
| [1.848 | 0.055 | 26.24 | 26.79 | 27 200 | 12 800 ] |
| | ±0.005 | ±2.48 | ±0.03 | | |
| [1.848 | 0.280 | 5.11 | 27.05 | 27 200 | 12 000 ] |
| | ±0.025 | ±0.78 | ±0.05 | | |
| 1.919 | 0.314 | 4.74 | 27.12 | 21 600 | 16 800 |
| | ±0.022 | ±0.34 | ±0.05 | | |
| 1.991 | 0.408 | 3.78 | 27.31 | 16 800 | 8800 |
| | ±0.038 | ±0.35 | ±0.11 | | |
| 2.277 | 0.495 | 3.56 | 27.64 | 16 800 | 12 000 |
| | ±0.044 | ±0.32 | ±0.10 | | |

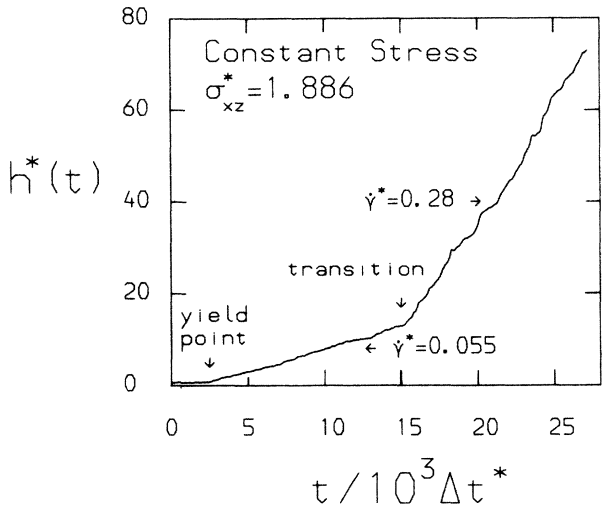


FIG. 1. Response of the soft-sphere crystal sample to a constant applied stress of $\sigma_{xz}^* = 1.886$ ($\sigma_{xz}^* = \sigma_{xz}V/Nk_bT$). The displacement of the periodic images, $h^*(t) = h(t)/\sigma$ [see Eq. (10)] plotted as a function of time. Note the yield point and the two distinct shearing phases.

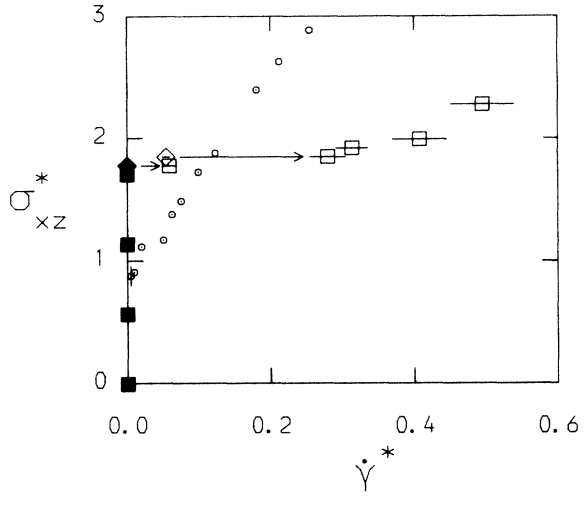


FIG. 2. The mean reduced shear rate [$\dot{\gamma}^* = \frac{1}{2}\dot{\gamma}\sigma(m/\epsilon)^{1/2}(\epsilon/k_bT)^{7/12}$] plotted against the applied stress ($\sigma_{xz}^*$) for the simulations of the 504-particle soft-sphere crystal. The open squares represent our data. The solid squares denote nonshearing points and diamonds have been used for the metastable points given in Table II. Also plotted, as circles, are the constant-shear-rate data of Evans (Ref. 14).

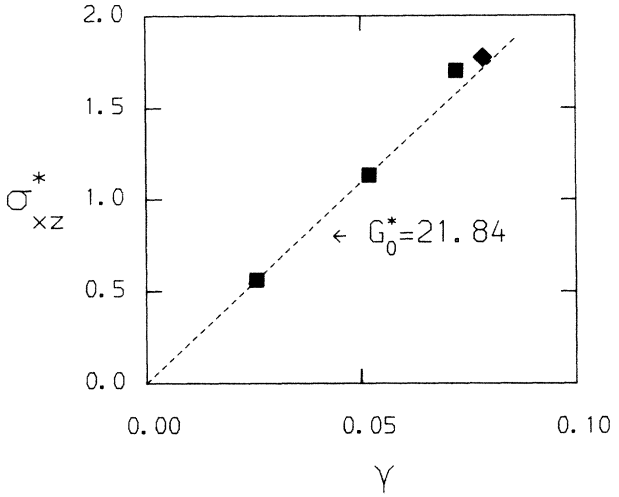


FIG. 3. The means strain ($\gamma$) plotted as a function of the applied stress for the nonshearing points. Notation as for Fig. 2. The dashed line is a fit of the first two points to the form $\sigma^*_{xz}=G_0^*\gamma$ with $G_0^*=21.84$.

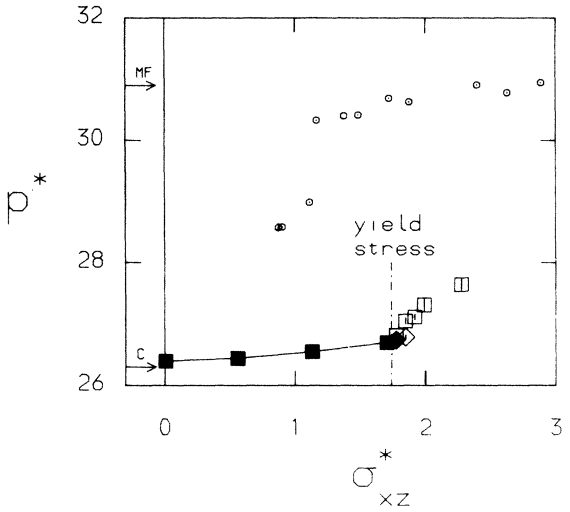


FIG. 4. The mean reduced pressure ($p^*=pV/Nk_bT$) plotted as a function of the applied stress. Notation as for Fig. 2. The dot-dashed line marks the value of the yield stress. The constant-shear-rate data of Evans (Ref. 14) is plotted as circles. The pressure of the equilibrium crystal ($C$) and the metastable fluid (MF) are marked by the horizontal arrows.

In Fig. 3 the time-averaged value of $\gamma$ is plotted against $\sigma^*_{xz}$ for the applied stresses up to and including the metastable point $\sigma^*_{xz}=1.776$. The lowest two stress points fit well to the form of Eq. (14) with a reduced shear modulus $G_0^*$ of 21.84. At the higher stresses it is clear nonlinearity occurs as the yield point is approached. In a narrow range of stress just in excess of $\sigma^0_{xz}$ it appears that there is a stable low-shear-rate—high-viscosity phase. This gives way to at least one higher-shear-rate—lower-viscosity phase for stresses $\geq 1.776$, more of which will be said in due course.

None of our stress-induced phases correspond with those observed previously in computer simulations.[14] This can also be seen in Fig. 4 where the pressure has been plotted as a function of the applied stress along with the data of Evans.[14] Below the yield stress our pressure data extrapolate smoothly back to that expected of the equilibrium crystal ($C$).[14] Even into the shearing regime the pressure increases are modest compared to those observed previously,[14] the latter being more characteristic of the metastable fluid (MF) at this density. There is clearly much less disruption of the crystal structure when the shear is directed along the (111) face. We believe that the "shear-induced melting"[14] was an artifact of a system in which particles are prevented from rearranging into stable shearing planes by the cubic shape of the MD cell.

Although the crystal and shear geometry used here more readily facilitate shearing, it should not be concluded that the results are devoid of artifacts. In Fig. 5 the nonconstrained off-diagonal elements of the stress tensor are plotted as a function of the applied stress. It can be seen that application of stress in the $xz$ plane causes the development of significant tangential components. Clearly the crystal would like to strain in the $xy$ and $yz$ directions but is constrained not to do so by the fixed cell geometry. Further evidence of this is available from the shear moduli. The modulus obtained from the stress-strain relationship $G_0^*=21.84$ which is significantly greater than $G_\infty$. Normally $G_0 \leq G_\infty$ so this also suggests that the direction in which the stress is initially applied is not that in which the crystal strains most easily.

The occurrence of these off-diagonal stresses below the yield point is probably related to the observed metastability of the fcc crystal *above* the yield point. Analysis of the structure and dynamics of the system reveals that the (111) crystal planes maintain their integrity throughout the simulations with no interchange of particles between

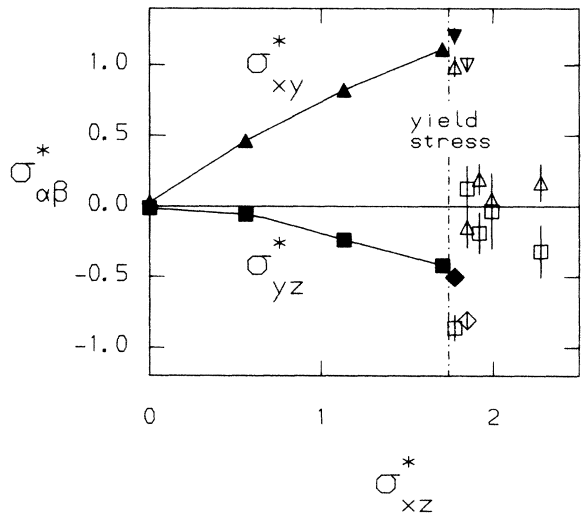


FIG. 5. The mean nonconstrained $xy$ (open triangles) and $yz$ (open squares) components of the stress tensor plotted against the applied stress. Solid triangles and squares represent nonshearing points and diamonds and inverted triangles denote the metastable points. The yield stress is shown dot-dashed line.

the layers in the $z$ direction. There is, however, a change in the registry of the layers from the *ABC* formation required of the fcc crystal, which coincides with the transition to the higher-shear-rate regime. At this point most of the layers slip into the *ABA* formation of a hexagonal-close-packed (hcp) structure and this is accompanied by the simultaneous collapse of the tangential stresses. This result suggests that hcp is the stable shearing geometry for the chosen applied stress although complete rearrangement is impossible in our nine-layer crystal sample. Clearly a more general method of controlling stress tensor elements is required (similar to the Rahman-Parinello method[5]) if the true response of different crystals to an arbitrary direction of shear is to be determined.

## CONCLUSIONS

We have demonstrated the practicability of a constant-stress NEMD method capable of following crystalline or fluid systems continuously through the straining to the flowing regimes. For a liquid phase simulation results from constant-stress and constant-strain-rate NEMD are in good agreement. Results obtained for stress applied to the (111) face of a small sample of a defect-free fcc soft-sphere crystal demonstrate the existence of a well-defined yield stress in the system and at least two stable shearing phases. However, our results are in marked contrast to those obtained previously[14] using constant shear applied to the (100) face. We find no evidence for the crystal melting into the normal shearing fluid phase even at shear rates twice those used in Ref. 14. At constant applied stress the properties of the equilibrium crystal are recovered as the stress tends to zero. The results show that shear-induced meting and other phase transitions can be merely artifacts introduced by the constraints placed on the system and by the small size and particular geometry of the MD cell.

## ACKNOWLEDGMENTS

We would like to acknowledge helpful discussions of this work with fellow attendees of a CECAM workshop, in particular Bill Hoover and Tony Ladd.

[1]W. G. Hoover, Annu. Rev. Phys. Chem. **34**, 103 (1983).
[2]W. G. Hoover, Physica **118A**, 51 (1983).
[3]D. J. Evans, Physica **118A**, 111 (1983).
[4]D. J. Evans and G. P. Morriss, Comput. Phys. Rep. **1**, 297 (1984).
[5]M. Parinello and A. Rahman, J. Appl. Phys. **52**, 7182 (1981).
[6]A. J. C. Ladd, Mol. Phys. **53**, 459 (1984).
[7]T. A. Andrea, W. C. Swope, and H. C. Anderson, J. Chem. Phys. **79**, 4576 (1983).
[8]D. J. Evans, J. Chem. Phys. **78**, 3297 (1983).
[9]D. Fincham and D. M. Heyes, Adv. Chem. Phys. **63**, 493 (1985).
[10]B. Quentrec, Mol. Phys. **46**, 707 (1982).
[11]B. C. Eu, J. Chem. Phys. **79**, 2315 (1983).
[12]*Dislocation Dynamics*, edited by A. R. Rosenfield, G. T. Hahn, A. L. Bement, and R. Jafee (McGraw-Hill, New York, 1968).
[13]W. G. Hoover, A. J. C. Ladd, and B. Moran, Phys. Rev. Lett. **48**, 1818 (1982).
[14]D. J. Evans, Phys. Rev. A **25**, 2788 (1982).
[15]L. V. Woodcock, Phys. Rev. Lett. **54**, 1513 (1985).
[16]R. Zwanzig and R. D. Mountain, J. Chem. Phys. **43**, 4464 (1965).
[17]D. Tabor, *Gases, Liquids and Solids* (Penguin, Glasgow, 1970), p. 160.